Combined Catalytic Action of Supported Cu and Au in Imine Production from Coupled Benzyl Alcohol and Nitrobenzene Reactions

Accepted Manuscript

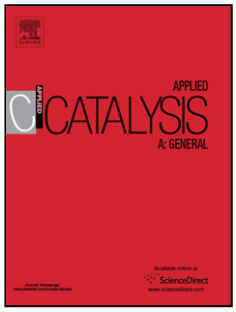

Title: Combined Catalytic Action of Supported Cu and Au in Imine Production from Coupled Benzyl Alcohol and Nitrobenzene Reactions

Authors: Maoshuai Li, Fernando Cárdenas-Lizana, Mark A. Keane

PII: S0926-860X(18)30143-1
DOI: https://doi.org/10.1016/j.apcata.2018.03.024
Reference: APCATA 16598

To appear in: *Applied Catalysis A: General*

Received date: 8-2-2018
Revised date: 20-3-2018
Accepted date: 22-3-2018

Please cite this article as: Li M, Cárdenas-Lizana F, Keane MA, Combined Catalytic Action of Supported Cu and Au in Imine Production from Coupled Benzyl Alcohol and Nitrobenzene Reactions, *Applied Catalysis A, General* (2010), https://doi.org/10.1016/j.apcata.2018.03.024

Combined Catalytic Action of Supported Cu and Au in Imine Production from Coupled Benzyl Alcohol and Nitrobenzene Reactions

Maoshuai Li, Fernando Cárdenas-Lizana and Mark A. Keane*

Chemical Engineering, School of Engineering and Physical Sciences,

Heriot-Watt University, Edinburgh EH14 4AS, Scotland

*corresponding author

Tel: +44(0)131 451 4719, e-mail: M.A.Keane@hw.ac.uk

Graphical Abstract

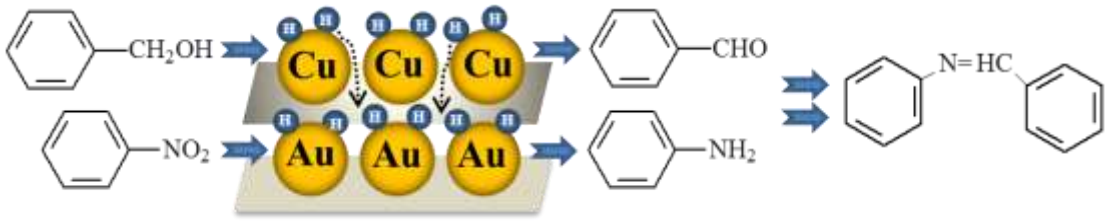

Highlights

1. Continuous single-pot imine synthesis from benzyl alcohol and nitrobenzene
2. Hydrogen ‘‘borrowing’’ strategy for sustainable imine production
3. Synergism between Cu and Au for full H_2 utilisation in cross-coupled reaction
4. Stable selective *N*-benzylideneaniline production over Au/TiO_2+Cu/SiO_2

Abstract

The feasibility of continuous gas phase coupling of benzyl alcohol dehydrogenation with nitrobenzene hydrogenation for imine (*N*-benzylideneaniline) synthesis over mixtures of Cu/SiO_2 and (TiO_2, MgO) supported Au catalysts has been established. The catalysts were characterised in terms of specific surface area, pore volume, TPR, H_2 chemisorption, STEM, XPS and TGA-DSC analysis. Au/TiO_2 prepared by deposition-precipitation exhibited a narrower particle size distribution (1-6 nm) and smaller mean (3.2 nm) than Au/MgO (1-15 nm, mean = 7.7 nm) prepared by impregnation. Dehydrogenation of benzyl alcohol (to benzaldehyde) over Cu/SiO_2 delivered a (ten-fold) higher rate than supported Au and Au/TiO_2 exhibited a higher H_2 chemisorption capacity and greater (by a factor of ten) nitrobenzene hydrogenation rate than Cu/SiO_2 and Au/MgO. Inefficient hydrogen utilisation is demonstrated for the cross-coupling reaction over Cu/SiO_2 alone and a temporal activity loss is linked to carbonaceous (benzoate) deposition (on the basis of XPS and TGA-DSC analysis). Incorporation of Au/TiO_2 (and Au/MgO) with Cu/SiO_2 increased the imine formation rate and

H_2 utilisation efficiency. The combination of Au/TiO_2 with Cu/SiO_2 served to circumvent Cu/SiO_2 deactivation, resulting in enhanced stability with a four-fold increase in imine production and full H_2 utilisation at Cu/Au = 10.

Keywords**:** reaction coupling; benzyl alcohol; nitrobenzene; imine; Cu/SiO_2; Au/TiO_2.

1. Introduction

Higher substituted imines are extensively used as intermediates in the manufacture of fine chemicals, pharmaceuticals and agrochemicals [1]. Conventional production draws on reductive amination (alkylation) of aldehydes/ketones with amines that are derived from the reduction of nitro-compounds at elevated H_2 pressures (4-12 bar) [2-4]. Hydrogen is not a naturally occurring feedstock and current production (*ca.* 95%) is fossil fuel based, notably by methane steam reforming and coal gasification [5]. Issues linked to sustainable H_2 production are now the driver for the search of more efficient routes to imines. Work to date has focused on batch liquid phase catalytic oxidation of amines [6] (*e.g.* benzylamine over Au [7] and Cu [8]) and oxidative condensation of alcohols with amines [9] (*e.g.* benzyl alcohol and aniline over Cu [10], Pd [11] and Au [12]) at (O_2/air) pressures up to 5 atm. The multi-step nature of the oxidative route where the amine reactant must be generated first is a decided drawback [13]. We propose to integrate the nitro- → amine reduction step (**Fig. 1**, step **(I)**) and reaction with aldehyde (step **(III)**) in a "one pot" imine production that circumvents multiple reactor operation. The alcohol dehydrogenation (step **(II)**) is used to generate aldehyde and hydrogen that is utilised in $–NO_2$ hydrogenation. This removes the requirement for an external supply of pressurised H_2 and can be step-changing in terms of sustainability and process efficiency.

Synthesis of imines *via* coupling of alcohol dehydrogenation with nitro-compound reduction has not been studied to any significant extent. The viability of batch liquid phase coupling of benzyl alcohol dehydrogenation (as hydrogen donor) with nitrobenzene hydrogenation has been demonstrated for reaction over $Mg_6Al_2(OH)_{16}CO_3$ supported Pd but amine (>7% yield) was generated as by-product [14]. Xiang *et al.* [15] have reported imine synthesis from nitrobenzene and furfural over Pd-Au/Al_2O_3 (with MeOH as hydrogen source). We can also flag work dealing with batch conversion of nitroarenes and benzaldehyde over iron powder (with HCl as hydrogen donor) [16] and nitrobenzene with benzyl alcohol over

TiO_2 supported Au-Pd and Ru-Pd [17]. A move from batch to continuous processing has significant benefits in terms of economics, high throughput and quality control. This has been identified as a priority for sustainable production in the pharmaceutical and fine chemical sectors [18]. Studies of continuous gas phase operation employing a hydrogen ‘‘borrowing’’ strategy have predominantly dealt with coupling of dehydrogenation and hydrogenation [19-22] with no report of cross-coupling of alcohols with nitro- reactants for imine synthesis. Baiker *et al*. [23,24] studied the formation of dimethyldodecylamine by gas phase conversion of dimethylamine and 1-dodecanol over Cu/Al_2O_3 and observed loss of activity and selectivity in the absence of an external hydrogen supply. Deactivation has been a feature of coupling reactions involving alcohols and amines over supported Cu and Ni catalysts and attributed to nitride formation, coking and amine deposition [25].

We have previously established the viability of hydrogen transfer (from 2-butanol dehydrogenation) for nitrobenzene reduction over Cu/SiO_2 [26]. In this study, we extend that work to evaluate feasible imine production in the absence of external H_2 using a combination of Cu/SiO_2 and supported Au catalysts with benzyl alcohol and nitrobenzene as reactants (**Fig. 1**). Nitroarene hydrogenation over supported Au shows a dependency on support reducibility [27], where Au on TiO_2 and MgO exhibited differences in chemoselective amine production rates [28]. We evaluate H_2 utilisation and catalyst stability as two critical considerations for sustainable imine production.

2. Experimental

2.1 Catalyst Preparation and Activation

Cu/SiO_2 was prepared by deposition-precipitation with NaOH (Riedel-de Haën, 99%) as precipitation agent. Silica powder (Sigma-Aldrich, 20 g) was dispersed in an aqueous solution of $Cu(NO_3)_2$ (Sigma-Aldrich, 99%, 0.03 M, 200 cm^3). The suspension was stirred (600 rpm) at ambient temperature for 1 h and NaOH (2 M) added dropwise until pH >10 to ensure full

deposition as $Cu(OH)_2$ [29]. The mixture was heated in air to 353 K with subsequent ageing for 4 h to facilitate homogeneous deposition [29]. The solid obtained was separated by filtration, washed with distilled water until pH = 7 and dried at 393 K. The dried sample was calcined in air (at 10 K min^{-1} to 723 K for 4 h) to generate a supported copper oxide (CuO) [29]. Gold on MgO (Sigma-Aldrich, 10 g) was prepared by impregnation with aqueous $HAuCl_4$ (Sigma-Aldrich, 99%, 5×10^{-2} M, 50 cm^3). The slurry was heated (at 2 K min^{-1}) to 353 K at 600 rpm and maintained in a He purge for 5 h. Gold on TiO_2 (P25, Degussa) was prepared by deposition-precipitation using urea (Riedel-de Haën, 99%) as basification agent. An aqueous solution of urea (100 fold excess) and $HAuCl_4$ (5×10^{-3} M, 400 cm^3) was added to the support (15 g) and the suspension stirred and heated to 353 K under reflux (2 K min^{-1}). The pH progressively increased to reach *ca.* 7 after 3-4 h as a result of thermal decomposition of urea. The solid was separated by filtration, washed with distilled water and dried in 45 cm^3 min^{-1} He at 373 K for 5 h. The catalyst precursors were sieved (ATM fine test sieves) to mean particle diameter = 75 μm. Prior to *ex situ* characterisation and catalytic testing, samples were activated in 60 cm^3 min^{-1} H_2 at 2-4 K min^{-1} to 523-545 K, held for 1-2 h and passivated at ambient temperature in 1% v/v O_2/He.

2.2 Catalyst Characterisation

Metal loading was determined by atomic absorption spectroscopy (Shimadzu AA-6650 spectrometer with an air-acetylene flame) analysis of the diluted extract in aqua regia (25% v/v HNO_3/HCl). Temperature programmed reduction (TPR) and H_2 chemisorption were conducted on the CHEM-BET 3000 (Quantachrome Instrument) unit with data acquisition/ manipulation using the TPR Win^{TM} software. The sample was loaded into a U-shaped Pyrex glass cell (3.76 mm i.d.) and heated in 17 cm^3 min^{-1} (Brooks mass flow controlled) 5% v/v H_2/N_2 at 2-4 K min^{-1} to 523-545 K. The activated samples were swept with 65 cm^3 min^{-1} N_2 for 1.5 h, cooled to

reaction temperature (498 K) and subjected to H_2 chemisorption by pulse (10 μl) titration. The effluent gas passed through a liquid N_2 trap and H_2 consumption was monitored by a thermal conductivity detector (TCD). In blank tests, there was no measurable H_2 uptake on the (SiO_2, TiO_2 or MgO) supports. Nitrogen adsorption-desorption isotherms were obtained using the Micromeritics Gemini 2390p system. Prior to analysis, the samples were outgassed at 423 K for 1 h in N_2. Total specific surface area (SSA) and cumulative pore volumes were obtained using standard BET and BJH analysis. Metal particle morphology (size and shape) was examined by scanning transmission electron microscopy (STEM, JEOL 2200FS field emission gun-equipped unit), employing Gatan Digital Micrograph 1.82 for data acquisition/manipulation. Samples for analysis were prepared by dispersion in acetone and deposited on a holey carbon/Cu grid (300 Mesh). Surface area weighted mean metal size (*d*) was based on a count of up to 800 nanoparticles according to

$$d = \frac{\sum_i n_i d_i^3}{\sum_i n_i d_i^2} \quad \textbf{(1)}$$

where n_i is the number of particles of diameter d_i. Thermogravimetric analysis (TGA) and differential scanning calorimetry (DSC) of the samples *pre*- and/or *post*-reaction were performed on a SDT Q600 simultaneous TGA/DSC analyser (TA Instrument) by monitoring temporal mass and heat flow changes with temperature. The samples (*ca.* 10 mg) were heated in 100 cm^3 min^{-1} air at 373 K for 1 h and ramped to 1073 K (at 20 K min^{-1}). Elemental (C, H and N) analysis for samples *pos*t-reaction was carried out on an Exeter CE-400 elemental analyser. X-ray photoelectron spectroscopic (XPS) analysis was conducted on an Axis Ultra instrument (Kratos Analytical) under ultra-high vacuum conditions (<10^{-8} Torr) with a monochromatic Al Kα radiation (1486 eV). The C1*s*, Cu 2$p_{3/2}$, Au 4$f_{5/2}$ and 4$f_{7/2}$, N1*s* and Si 2*p* spectra were collected. Characteristic Cu 2$p_{3/2}$ binding energies (BE) for metallic Cu and CuO are 932.8 eV [30] and 934.0 eV [31], respectively. Values in the 83.6-84.2 eV and 87.2-

88.4 eV ranges for $4f_{7/2}$ and $4f_{5/2}$ levels have been reported elsewhere [32] for metallic Au. We define adventitious carbon as any carbon associated with air exposed samples [33]. The C1*s* profile for this adventitious carbon is characterised by a principal peak at 284.5 eV, indicative of alkyl species (C–C, C–H) [34], and was used as an internal standard to compensate for charging effects. The spectra were calibrated against the Si 2*p* (of SiO_2, BE = 103.5 eV) [35] and fitted with abstraction of the Shirley background using the Gaussian-Lorentzian function in XPSPEAK 41.

2.3 Catalytic Procedure

Reactions (stand-alone benzyl alcohol dehydrogenation and nitrobenzene hydrogenation and cross-coupling) were carried out at ambient pressure *in situ* after activation in a continuous flow fixed bed vertical glass reactor (i.d. = 15 mm) at 423-523 K. A layer of borosilicate glass beads served as preheating zone, ensuring that the reactant(s) (benzyl alcohol and/or nitrobenzene) was (were) vaporised and reached reaction temperature before contacting the catalyst bed. Isothermal conditions (±1 K) were maintained by diluting the catalyst with ground glass (75 μm) and continuously monitored by a thermocouple inserted in a thermowell within the catalyst bed. The reactant(s) was (were) delivered to the reactor *via* a glass/teflon air-tight syringe and teflon line using a microprocessor controlled infusion pump (Model 100 kd Scientific). Dehydrogenation of benzyl alcohol and hydrogenation of nitrobenzene were tested separately in a co-current flow of N_2 with benzyl alcohol ($GHSV = 1.0 \times 10^4$ h^{-1}, molar metal to reactant feed rate $n_{metal}/F = 3.8 \times 10^{-3} – 5.0 \times 10^{-2}$ h) and H_2 with nitrobenzene ($GHSV = 1.0 \times 10^4$ h^{-1}, $n_{metal}/F = 8.0 \times 10^{-3} – 1.2 \times 10^{-2}$ h), respectively. The coupled reaction was carried out in N_2 ($GHSV = 2.0 \times 10^3$ h^{-1}, $n_{metal}/F = 1.2 \times 10^{-1} – 3.6 \times 10^{-1}$ h). In blank tests, passage of each reactant through the empty reactor or over the (SiO_2, TiO_2 or MgO) support alone did not result in any detectable conversion. The reactor effluent was condensed in a liquid nitrogen trap

for subsequent analysis using a Perkin-Elmer Auto System XL gas chromatograph equipped with a programmed split/splitless injector and a flame ionization detector, employing a DB-1 (50 m × 0.33 mm i.d., 0.20 μm film thickness) capillary column (J&W Scientific). Data acquisition and manipulation were performed using the TurboChrom Workstation Version 6.3.2 (for Windows) chromatography data system. Benzyl alcohol (Riedel-de Haën, ≥99%), benzaldehyde (Fluka, ≥98%), nitrobenzene (Riedel-de Haën, ≥99%), aniline (Sigma-Aldrich, ≥99%), toluene (Sigma-Aldrich, 99%), *N*-benzylideneaniline (Sigma-Aldrich, 99%) and *N*-benzylaniline (Sigma-Aldrich, 99%) were used as received without further purification. The (H_2, N_2, O_2 and He) gases were of high purity (BOC, >99.98 %). Reactant (i) fractional conversion (X_i) is defined by

$$X_{\mathrm{i}} = \frac{[reactant]_{\mathrm{i,\,in}} - [reactant]_{\mathrm{i,\,out}}}{[reactant]_{\mathrm{i,\,in}}} \qquad \textbf{(2)}$$

and composition (N_j) with respect to product j by

$$N_{\mathrm{j}}\,(\%) = \frac{[Product]_{\mathrm{j,out}}}{\sum_{\mathrm{j=1}}^{\mathrm{n}} [Product]_{\mathrm{j,out}}} \times 100 \qquad \textbf{(3)}$$

where subscripts “in” and “out” refer to the inlet and outlet gas streams, respectively. Activity is quantified in terms of reaction rate (R, mmol mol_{metal}^{-1} h^{-1}), determined from time on-stream measurements as described elsewhere [28]. Repeated reaction with different samples from the same batch of catalyst delivered raw data reproducibility and mass balances within ±5%.

3. Results and Discussion

3.1 Cu/SiO_2: Characterisation (*Pre*-reaction) and Catalytic Response in Stand-Alone and Cross-Coupling Reactions.

The physicochemical characteristics of Cu/SiO_2 given in **Table 1** reveal a lower SSA than the silica support (223 $m^2\ g^{-1}$) but a comparable pore volume (SiO_2 = 0.35 $cm^3\ g^{-1}$). Activation by TPR (**Fig. 2(AI)**) generated a positive (H_2 consumption) peak at the final isothermal hold (545 K) where the H_2 consumed matched the requirements for $Cu^{2+} \rightarrow Cu^0$ reduction (**Table 1**). Hydrogen chemisorption capacity is a critical catalyst characteristic for hydrogenation applications. We have noted previously low H_2 uptake on Cu/SiO_2 (25 µmol g_{Cu}^{-1}) at ambient temperature [26] that can be linked to the filled *d* band [36]. Hydrogen adsorption on Cu is an activated process, where Cu/SiO_2 showed higher uptake at 498 K (**Table 2**). This value is appreciably lower than that recorded for silica supported hydrogenation metals such as Pd (1650 µmol g_{Pd}^{-1}) [37] and Ni (614 µmol g_{Ni}^{-1}) [38]. STEM analysis (**Fig. 2(AII)**) revealed the presence of Cu particles at the nano-scale (1-6 nm, **Fig. 2(AIII)**) with a surface area weighted mean of 3.1 nm.

The coupled dehydrogenation-hydrogenation system requires a higher dehydrogenation rate relative to hydrogenation to ensure sufficient H_2 supply for reaction. We first examined separately the dehydrogenation of benzyl alcohol (in N_2) and hydrogenation of nitrobenzene (using an external H_2 supply) over Cu/SiO_2. Benzyl alcohol dehydrogenation generated benzaldehyde (**Fig. 1**, step **(II)**) as the sole product over the 423-498 K temperature range. Toluene formation (≤10% selectivity, step **(V)** in **Fig. 1**) was observed for reaction at 523 K. Full selectivity to the target benzaldehyde at $T < 498$ K is consistent with that reported for K-Cu/TiO_2 [39]. Benzyl alcohol hydrogenolysis over Cu/MgO required temperatures ≥513 K [40]. We have previously established pseudo-first order kinetics for catalytic dehydrogenation (of 2-butanol) [26] and nitroarene hydrogenation [41]. The associated Arrhenius plots (423-

498 K) using the extracted pseudo-first order rate constants (*k*) are presented in **Fig. 3** with an associated apparent activation energy for the dehydrogenation reaction of 37 kJ mol^{-1}. We could not find any reported activation energy for benzyl alcohol conversion to benzaldehyde. The value (20 kJ mol^{-1}) recorded for *n*-octyl alcohol dehydrogenation (over Cu/Al_2O_3-MgO) is lower [42]. Nitrobenzene hydrogenation (**Fig. 1**, step **(I)**) over Cu/SiO_2 resulted in exclusive production of aniline with no hydrodenitrogenation or aromatic ring reduction. The apparent activation energy (32 kJ mol^{-1}, **Fig. 3**) falls within the range (12-54 kJ mol^{-1}) reported for reaction over supported Ag [43], Pd [44] and Ni [45] catalysts.

The prerequisite for our coupled system to work in the absence of an external H_2 supply (*i.e.* in N_2) is that the quantity of hydrogen generated in the benzyl alcohol → benzaldehyde step meets the stoichiometry (=3) for the nitrobenzene → aniline transformation (**Fig. 1**, steps **(I-III)**). A four-fold higher benzyl alcohol dehydrogenation rate than nitrobenzene hydrogenation satisfies this requirement. Temporal variations in conversion for reaction at 498 K (where the highest selective benzyl alcohol dehydrogenation rate was achieved) are shown in **Fig. 4**. The coupled reaction generated imine and benzaldehyde with no detectable hydrogenolysis to toluene (step **(V)**, **Fig. 1**) and/or amine from further hydrogenation of imine (**step (IV)**). This represents the first reported continuous imine synthesis *via* coupled alcohol dehydrogenation and nitroarene hydrogenation without external H_2. Imine generation in N_2 demonstrates that the catalyst "borrows" hydrogen generated from the alcohol dehydrogenation (step **(II)**, **Fig. 1**) with an "auto-transfer" in the catalytic reduction of nitrobenzene to aniline (step **(I)**). As aniline is a strong nucleophile, it undergoes facile condensation with benzaldehyde to the target imine (step **(III)**) [46]. This represents innovation in process intensification and enhanced sustainability over conventional multi-stepped methodologies that require an external H_2 supply [2,3,8,10,47]. A temporal decline in conversion was observed (**Fig. 4**). Baiker [23] studying the gas phase (T = 510 K, P = 1 atm) cross-coupling alkylation

of dimethylamine with 1-dodecanol over Cu/Al_2O_3 reported a severe loss of activity that was ascribed to the formation of copper nitride (Cu_3N) from NH_3 generated by the disproportionation of dimethylamine.

Temperature is a critical process variable that influences reaction rate and product distribution [48]. Imine formation rate (R), molar (benzaldehyde/imine) product ratio ($N_{\text{-C=O}}/N_{\text{-C=N}}$) and hydrogen utilisation efficiency, expressed as the ratio of mol H_2 generated from benzyl alcohol dehydrogenation to mol imine produced (H_2/–C=N) are presented as a function of temperature (448-498 K) in **Table 2**. An increase in temperature at the reaction stoichiometry (inlet alcohol/nitroarene (–OH/–NO_2) = 3) resulted in a greater imine formation rate (by a factor of 50) with a higher imine content in the product and improved H_2 utilisation. The increased reaction rate can be attributed to greater hydrogen availability (from the Arrhenius plot in **Fig. 3**) in tandem with improved H_2 chemisorption capacity of Cu/SiO_2 at higher temperatures as determined from H_2 titration measurements. It should however be noted that product ratio ($N_{\text{-C=O}}/N_{\text{-C=N}}$) was greater than that (= 2) shown in the reaction scheme (**Fig. 1**) and H_2/–C=N exceeded the stoichiometry requirement (= 3) for full H_2 utilisation, necessitating further process optimisation.

It has been demonstrated that –OH/–NO_2 is critical in determining product distribution in liquid phase cross-coupling [14]. A higher –OH/–NO_2 served to increase the imine formation rate (**Table 2**). This suggests competition between nitrobenzene and benzyl alcohol for surface sites where higher alcohol content in the feed favours alcohol dehydrogenation with greater hydrogen release that contributed to the hydrogenation step. Shimizu *et al*. [49] proposed that dehydrogenation was rate determining in the coupled reaction of aniline with benzyl alcohol in N_2 for amine (*N*-benzylaniline) synthesis over Ni/Al_2O_3. Hydrogen utilisation (H_2/–C=N) and product ratio ($N_{\text{-C=O}}/N_{\text{-C=N}}$) were largely insensitive to variations in –OH/–NO_2 (**Table 2**). Incomplete H_2 utilisation can be linked to the low hydrogenation activity of Cu catalysts.

Incorporation of a second metal with greater hydrogenation capability can serve as a means of increasing imine production. The second metal must not promote side-reactions (benzyl alcohol hydrogenolysis and imine hydrogenation). Supported Pd, Pt and Ni exhibit high activity in the reduction of unsaturated functions (*e.g.* $–NO_2$ and –C=O) but promote hydrogenolysis, generating a range of by-products (*e.g.* toluene) [50,51]. In contrast, nano-scale Au has displayed unique chemoselectivity for hydrogenation of $–NO_2$ in the presence of other reactive groups (*e.g.* –C=O) [3]. Supported Au was chosen in this study as a suitable candidate to improve hydrogen utilisation directed at enhanced imine production rates.

3.2 Supported Au: Characterisation (*Pre*-reaction) and Catalytic Response in Stand-alone Dehydrogenation and Hydrogenation Reactions.

It has been shown that $–NO_2$ adsorption/activation at TiO_2 and Au-TiO_2 interface sites deliver enhanced selective nitroarene reduction rates [52]. In order to probe possible support effects, we also examined the performance of Au/MgO as an additive in the cross-coupled reaction. The TPR profile of Au/TiO_2 (**Fig. 2(BI)**) exhibits a single H_2 consumption peak (T_{max} = 378 K) that exceeded the amount needed for Au^{3+} reduction to Au^0 (**Table 1**), suggesting partial support reduction [53]. Reduction of Au/MgO (**Fig. 2(CI)**) generated a weak and broad higher temperature (T_{max} = 510 K) signal, where H_2 consumption (**Table 1**) was appreciably lower than that required for precursor reduction. This can be ascribed to reduction *pre*-TPR, during catalyst synthesis and drying [54]. Representative STEM images **(BII**, **CII)** and particle size distributions **(BIII**, **CIII)** are provided in **Fig. 2**. Au/TiO_2 is characterised by a narrow particle size range (1-6 nm) and a mean (3.2 nm) close to that of Cu/SiO_2. In contrast, Au/MgO bore larger Au particles (1-15 nm, mean = 7.7 nm) that is a consequence of synthesis by impregnation, which results in weaker metal-support interaction and agglomeration during thermal treatment [55]. Gold particle size <10 nm has been identified as critical for activity in hydrogenation applications [36]. A significantly higher H_2 chemisorption capacity was

recorded for Au/TiO_2 relative to Au/MgO (**Table 1**). This can be linked to the smaller Au particle size [56] and a contribution due to the $Au\text{-}TiO_2$ interface [57] that facilitates H_2 activation/dissociation. The performance of Au/TiO_2 and Au/MgO can be assessed against Cu/SiO_2 in stand-alone benzyl alcohol dehydrogenation and nitrobenzene hydrogenation in **Fig. 5**. The results establish lower (by an order of magnitude) dehydrogenation rates for the two Au catalysts (**Fig. 5(A)**). Negligible activity for gas phase alcohol dehydrogenation over supported Au is consistent with results for ethanol dehydrogenation over Au/SiO_2 at $T < 523$ K [58]. Au/TiO_2 delivered a significantly higher nitrobenzene hydrogenation rate than Cu/SiO_2 and Au/MgO (**Fig. 5(B)**), which correlates with H_2 chemisorption capacity (**Table 1**).

3.3 Cu + Au Physical Mixtures: Catalytic Response in Cross-Coupled Reactions.

We first assessed the catalytic action of mixed (Cu + Au) catalysts, varying the Cu/Au molar ratio (10, 20 and 80). The results are presented in **Fig. 6** and **Table 3** where benzaldehyde and the target *N*-benzylideneaniline were the only detected products. Imine production was enhanced on incorporating Au/TiO_2 with Cu/SiO_2 with a rate increase at higher Au content (Cu/Au from 80 to 10). This demonstrates the contribution of Au/TiO_2 to harness the hydrogen (generated from dehydrogenation, **Fig. 1**, step **(II)**) and promote nitroarene reduction (step **(I)**) with subsequent condensation (aniline + aldehyde) to imine (step **(III)**). We envision a synergism between Au and Cu that is illustrated in **Fig. 7**. The supported Cu phase promotes alcohol dehydrogenation with hydrogen abstraction (step **(I)**). Fridman *et al.* [59] have proposed a two-step H abstraction mechanism for Cu catalysed cyclohexanol dehydrogenation. Interaction between metal and abstracted hydrogen results in the formation of transient (Ru-H [60], Ag-H [46] and Ni-H [49]) species. Hydrogen on Cu sites (Cu-H) can "spillover" across the $Cu\text{-}SiO_2$ interface, the physical interface with Au/TiO_2 and onto Au sites (step **(II)**) [61] with auto-transfer in the catalytic conversion of nitrobenzene to aniline (step **(III)**) and

subsequent condensation (step **(IV)**). Further hydrogenation of imine to *N*-benzylaniline was not observed. This may be due to competition with nitrobenzene for surface hydrogen.

We obtained full hydrogen utilisation (H_2/–C=N = 3) and imine formation ($N_{\text{-C=O}}/N_{\text{-C=N}}$ = 2) over Cu/SiO_2 + Au/TiO_2 at Cu/Au = 10. This represents unprecedented performance in terms of atom efficiency and hydrogen usage when compared with conventional pressurised batch liquid phase reactions. Activity and selectivity in the coupled reactions over the physical mixture were invariant (at Cu/Au = 10) for up to 6 h on-stream (**Fig. 6(A)**), which is a marked improvement in stability relative to Cu/SiO_2 (**Fig. 4**). We could find no published study of catalytic coupled reactions over physical combinations of Cu+Au catalysts. We should note work where mixtures of (graphite) supported Pd (or Pt) with supported bimetallic Fe-Ce exhibited higher stability and activity relative to the individual catalysts in the hydrogenation-isomerisation of 1,3-butadiene to butane [62]. Incorporation of Au/MgO with Cu/SiO_2 (**Table 3**, **Fig. 6(B)**) also served to enhance the imine production rate with increasing Au content (Cu/Au = 20 → 10). This is again indicative of a cooperative effect in terms of alcohol dehydrogenation at Cu sites with hydrogen release and use in–NO_2 reduction on Au/MgO. The promotional effect was not as significant as that observed with Au/TiO_2, which exhibited higher nitrobenzene hydrogenation activity (**Fig. 5(B)**).

3.4 Cu/SiO_2 *vs.* Cu/SiO_2 + Au/TiO_2: Catalyst Characterisation (*Post*-reaction)

Given the decline in activity with time on-stream for Cu/SiO_2 (**Fig. 4**), we subjected a spent sample to characterisation measurements in order to identify the possible cause for deactivation. We also carried through the same analyses for a spent Au/TiO_2 + Cu/SiO_2 (Cu/Au = 10) physical mixture that delivered full conversion/hydrogen utilisation over 6 h on-stream (**Fig. 6(A)**). Catalyst deactivation in reactions involving alcohols and amines (or nitro-compounds) has been ascribed to active site occlusion/poisoning (nitride formation [23], coke

[63] and amine/nitro-compound deposition [25]) and/or changes to the oxidation state of the active metal [64]. Analysis by XPS provides information on surface composition and the chemical/electronic state of the supported metal phase. Spectra over the C1*s* **(A)** and Cu $2p_{3/2}$ **(B)** binding energy (BE) regions are shown in **Fig. 8**. The C1*s* profile for unused Cu/SiO_2 **(AI)** exhibited a contribution due to adventitious carbon (BE = 284.5 eV) with a secondary peak (BE = 286.1 eV) corresponding to C–OH or C–O–C [34]. An additional peak at 288.7 eV for spent Cu/SiO_2 **(AII)** can be tentatively linked to the carboxyl functionality in benzoate species (BE = 288.6-289.1 eV) [65]. The Cu $2p_{3/2}$ spectrum for the passivated unused Cu/SiO_2 **(BI)** presents a principal peak at BE = 933.2 eV characteristic of electron deficient copper ($Cu^{\delta+}$ = 933.0-933.6 eV) [66]. The spectrum also shows a secondary peak at higher BE (934.1 eV) that corresponds to CuO (BE = 934.0 eV [31]) and may be due to surface Cu oxidation during passivation [67]. *Post*-reaction **(BII)**, a peak at higher BE (936.5 eV) suggests a surface ionic Cu species [67,68] that can be attributed to copper benzoate formation. The formation of a surface benzoate has been proposed elsewhere [69] for benzaldehyde hydrogenation over oxide (SiO_2, TiO_2, ZrO_2 and CeO_2) supported Cu under similar reaction conditions (T = 373-623 K). The occurrence of Cu benzoate resulting from surface reaction of benzaldehyde with water (release from $–NO_2$ reduction) can reduce the number of available active sites and inhibit benzyl alcohol dehydrogenation, limiting hydrogen generation and subsequent nitrobenzene reduction/imine formation. The spectrum for used Cu/SiO_2 over the N1*s* region (396-400 eV, not shown) did not present any detectable signals. We have no evidence for the formation of copper nitride and/or surface nitrogenous species (T = 510 K, P = 1 atm) as was proposed elsewhere [23].

The XPS profile of the (Au + Cu) physical mixture *post*-reaction (**Fig. 8(AIII)**) exhibits a C1*s* peak at 287.8 eV that falls within the BE range (287.3-287.9 eV) reported for –C=O species [70-72] and can be assigned to surface benzaldehyde. Liu and co-authors [71] attributed a C1*s*

signal at 287.8 eV to residual aldehyde on surface copper during furfural hydrogenation. In the Cu $2p_{3/2}$ BE range (**Fig. 8(BIII)**), peaks characteristic of $Cu^{\delta+}$ and CuO were observed with no signal at BE > 936 eV for Au/TiO_2 + Cu/SiO_2. The comparison of XPS profiles for the spent Au/TiO_2 + Cu/SiO_2 and Cu/SiO_2 suggests the occurrence of surface benzaldehyde and benzoate species, respectively. Suppressed benzaldehyde → benzoate transformation results from the addition of Au/TiO_2. The incorporation of Au/TiO_2 with Cu/SiO_2 provides a more efficient site for nitrobenzene hydrogenation and aniline condensation with benzaldehyde (**Fig. 7**). This can ameliorate Cu deactivation as benzaldehyde reaction and $–NO_2$ reduction (with H_2O generation) proceeds at Au sites. The BE for Au $4f_{7/2}$ (83.2 ± 0.2 eV) and Au $4f_{5/2}$ (86.7 ± 0.2 eV) were lower than the reference Au^0 (84.0 eV and 87.8 eV) [73], suggesting the formation of an electron rich ($Au^{\delta-}$) phase as a result of electron donation from TiO_2 [74]. There was no measurable difference in Au BE *pre*- and *post*-reaction (**Fig. S1**, Supplementary Material).

The possible formation of carbonaceous deposits was further evaluated by TGA-DSC and elemental (C, H and N) analysis; the results are presented in **Fig. 9**. *Pre*-reaction, Cu/SiO_2 **(I)** and Cu/SiO_2 + Au/TiO_2 **(II)** exhibited a similar (2-3% w/w) mass loss at $T \leq 373$ K due to water release (**Fig. 9(A)**). Both spent samples displayed an additional higher temperature mass loss that can be attributed to combustion of carbonaceous species [63]. Elemental analysis (see inset Table in **Fig. 9(A)**) revealed a higher carbon content on the spent Cu/SiO_2 compared with the physical mixture. There was no measurable nitrogen, consistent with XPS results. The DSC profile of the spent Cu/SiO_2 (**Fig. 9(B)**) exhibited two exothermic mass losses (at 602 K and 702 K) during temperature programmed oxidation, indicative of different structural carbon deposits. The lower temperature exothermic mass loss matches that (553-613 K) corresponding to combustion of amorphous aromatic carbonaceous species [75,76]. Based on the DSC work of Siqueira *et al.* [77], the exothermic mass loss at higher temperature can be attributed to combustion of (copper) benzoate species. The DSC profile for the used Cu/SiO_2 + Au/TiO_2

mixture presents a principal mass loss at a lower temperature (582 K) with a secondary shoulder at 690 K. This is indicative of limited deposition of surface benzoate as suggested by XPS.

4. Conclusions

We have established the viability of ‘‘hydrogen-free’’ imine (*N*-benzylideneaniline) production *via* continuous gas phase cross-coupling of benzyl alcohol dehydrogenation with nitrobenzene hydrogenation and condensation over physical mixtures of supported Cu and Au catalysts. Dehydrogenation of benzyl alcohol to benzaldehyde over Cu/SiO_2 (mean Cu size = 3.1 nm) delivered a ten-fold higher rate than Au/TiO_2 (mean Au size = 3.2 nm). The latter exhibited significantly greater H_2 chemisorption capacity and nitrobenzene hydrogenation rate. Reaction over Cu/SiO_2 promoted cross-coupling to imine where an increase in temperature and inlet reactant alcohol/nitroarene ratio (–OH/–NO_2) served to enhance imine formation. The Cu catalyst suffered a severe temporal decline in activity linked to carbon (benzoate species from XPS and TGA-DSC measurements) deposition. Low hydrogen utilisation is due to the limited hydrogenation capacity of Cu. Incorporation of Au/TiO_2 with Cu/SiO_2 resulted in (4-fold) higher imine production rate with full hydrogen utilisation at Cu/Au = 10. This is the result of synergism between Cu and Au where hydrogen release from benzyl alcohol dehydrogenation on Cu is transferred to Au for nitrobenzene reduction (to aniline) and subsequent condensation with benzaldehyde to the imine. The promotional effect of Au/TiO_2 was greater than that observed with the addition of Au/MgO due to the greater H_2 chemisorption capability and –NO_2 reduction capacity of Au/TiO_2. Coupled reaction over Cu+Au exhibited stable performance with time on-stream where hydrogenation and condensation at Au sites circumvents Cu deactivation. Our results establish the feasibility of continuous stable gas phase imine synthesis using a ‘‘hydrogen borrowing’’ strategy over combined supported Cu and Au catalysts.

Acknowledgements

This work was financially supported by the Overseas Research Students Award Scheme (ORSAS) and in part by a grant from EPSRC (EP/M029476/1). We also acknowledge EPSRC support for free access to the XPS facility at the University of Newcastle and are grateful to J. F. Portoles and Dr. Y. Hao for their contributions to XPS analysis and catalyst preparation.

References

[1] Y. Wang, M. Mo, K. Zhu, C. Zheng, H. Zhang, W. Wang, Z. Shao, Nat. Comm. 6 (2015) 1-9.

[2] R. D. Patil, S. Adimurthy, Asian J. Org. Chem. 2 (2013) 726-744.

[3] L. L. Santos, P. Serna, A. Corma, Chem. A Eur. J. 15 (2009) 8196-8203.

[4] P. N. Scheller, M. Lenz, S. C. Hammer, B. Hauer, B. M. Nestl, ChemCatChem 7 (2015) 3239-3242.

[5] I. Dincer, C. Acar, Int. J. Hydrogen Energy 40 (2015) 11094-11111.

[6] P. Sudarsanam, B. Mallesham, A. Rangaswamy, B. G. Rao, S. K. Bhargava, B. M. Reddy, J. Mol. Catal. A: Chem. 412 (2016) 47-55.

[7] C. K. P. Neeli, R. K. Marella, S. Ganji, K. S. R. Rao, D. R. Burri, J. Chem. Technol. Biotechnol. 90 (2015) 1657-1664.

[8] L. Al-Hmoud, C. W. Jones, J. Catal. 301 (2013) 116-124.

[9] B. Chen, L. Y. Wang, S. Gao, ACS Catal. 5 (2015) 5851-5876.

[10] H. W. Tian, X. C. Yu, Q. Li, J. X. Wang, Q. Xu, Adv. Synth. Catal. 354 (2012) 2671-2677.

[11] M. Ousmane, G. Perrussel, Z. Yan, J. M. Clacens, F. de Campo, M. Pera-Titus, J. Catal. 309 (2014) 439-452.

[12] H. Sun, F.-Z. Su, J. Ni, Y. Cao, H.-Y. He, K.-N. Fan, Angew. Chem. Int. Ed. 48 (2009) 4390-4393.

[13] M. T. Schuemperli, C. Hammond, I. Hermans, ACS Catal. 2 (2012) 1108-1117.

[14] J. Chen, S. J. Huang, J. Lin, W. P. Su, Appl. Catal. A: Gen. 470 (2014) 1-7.

[15] Y. Xiang, Q. Meng, X. Li, J. Wang, Chem. Commun. 46 (2010) 5918-5920.

[16] A. L. Korich, T. S. Hughes, Synlett. 16 (2007) 2602-2604.

[17] M. Sankar, Q. He, S. Dawson, E. Nowicka, L. Lu, P. C. A. Bruijnincx, A. M. Beale, C. J. Kiely, B. M. Weckhuysen, Catal. Sci. Technol. (2016) 5473-5482.

[18] R. J. Giraud, P. A. Williams, A. Sehgal, E. Ponnusamy, A. K. Phillips, J. B. Manley, ACS Sust. Chem. Eng. 2 (2014) 2237-2242.

[19] A. Malaika, M. Kozłowski, Chem. Eng. J. 171 (2011) 1348-1355.

[20] Y.-L. Zhu, J. Yang, G.-Q. Dong, H.-Y. Zheng, H.-H. Zhang, H.-W. Xiang, Y.-W. Li, Appl. Catal. B: Environ. 57 (2005) 183-190.

[21] B. M. Nagaraja, A. H. Padmasri, B. D. Raju, K. S. R. Rao, J. Mol. Catal. A: Chem. 265 (2007) 90-97.

[22] B. M. Nagaraja, A. H. Padmasri, B. D. Raju, K. S. R. Rao, Int. J. Hydrogen Energy 36 (2011) 3417-3425.

[23] A. Baiker, Ind. Eng. Chem. Prod. Res. Dev. 20 (1981) 615-618.

[24] A. Baiker, D. Monti, Y. S. Fan, J. Catal. 88 (1984) 81-88.

[25] G. Guillena, D. J. Ramon, M. Yus, Chem. Rev. 110 (2010) 1611-1641.

[26] M. Li, Y. Hao, F. Cárdenas-Lizana, H. H. P. Yiu, M. A. Keane, Top. Catal. 58 (2015) 149-158.

[27] T. Mitsudome, K. Kaneda, Green Chem. 15 (2013) 2636-2654.

[28] M. Li, X. Wang, Y. Hao, F. Cárdenas-Lizana, M. A. Keane, Catal. Today 279 (2017) 19-28.

[29] Z. Huang, F. Cui, J. Xue, J. Zuo, J. Chen, C. Xia, Catal. Today 183 (2012) 42-51.

[30] J. P. Espinós, J. Morales, A. Barranco, A. Caballero, J. P. Holgado, A. R. González-Elipe, J. Phys. Chem. B 106 (2002) 6921-6929.

[31] J. Gong, H. Yue, Y. Zhao, S. Zhao, L. Zhao, J. Lv, S. Wang, X. Ma, J. Am. Chem. Soc. 134 (2012) 13922-13925.

[32] A. M. Visco, F. Neri, G. Neri, A. Donato, C. Milone, S. Galvagno, Phys. Chem. Chem. Phys. 1 (1999) 2869-2873.

[33] T. L. Barr, S. Seal, J. Vac. Sci. Technol. A 13 (1995) 1239-1246.

[34] M. C. Biesinger, B. P. Payne, A. P. Grosvenor, L. W. M. Lau, A. R. Gerson, R. S. Smart, Appl. Surf. Sci. 257 (2011) 2717-2730.

[35] J. Kleiman, M. Tagawa, Y. Kimoto, Protection of Materials and Structures from the Space Environment, Springer, Berlin, 2013.

[36] G. C. Bond, C. Louis, D. T. Thompson, Catalysis by Gold, Imperial College Press, London, 2006.

[37] S. Jujjuri, M. A. Keane, Chem. Eng. J. 157 (2010) 121-130.

[38] K.V. Murthy, P. M. Patterson, G. Jacobs, B. H. Davis, M. A. Keane, J. Catal. 223 (2004) 74-85.

[39] J. Fan, Y. H. Dai, Y. L. Li, N. F. Zheng, J. F. Guo, X. Q. Yan, G. D. Stucky, J. Am. Chem. Soc. 131 (2009) 15568-15569.

[40] R. K. Marella, C. K. P. Neeli, S. R. R. Kamaraju, D. R. Burri, Catal. Sci. Technol. 2 (2012) 1833-1838.

[41] F. Cárdenas-Lizana, S. Gómez-Quero, C. J. Baddeley, M. A. Keane, Appl. Catal. A: Gen. 387 (2010) 155-165.

[42] M. E. Crivello, C. F. Pérez, S. N. Mendieta, S. G. Casuscelli, G. A. Eimer, V. R. Elías, E. R. Herrero, Catal. Today 133 (2008) 787-792.

[43] G. D. Yadav, R. K. Mewada, Chem. Eng. J. 221 (2013) 500-511.

[44] I. I. Obraztsova, N. K. Eremenko, Y. N. Velyakina, Kinet. Catal. 49 (2008) 401-406.

[45] J. Wang, Z. Yuan, R. Nie, Z. Hou, X. Zheng, Ind. Eng. Chem. Res. 49 (2010) 4664-4669.

[46] H. Liu, G.-K. Chuah, S. Jaenicke, J. Catal. 292 (2012) 130-137.

[47] A. Srivani, P. S. S. Prasad, N. Lingaiah, Catal. Lett. 142 (2012) 389-396.

[48] V. Zamlynny, L. Kubelková, E. Babůrek, K. Jiratová, J. Nováková, Appl. Catal. A: Gen. 169 (1998) 119-125.

[49] K. Shimizu, N. Imaiida, K. Kon, S. Siddiki, A. Satsuma, ACS Catal. 3 (2013) 998-1005.

[50] A. Corma, P. Serna, Science 313 (2006) 332-334.

[51] N. Perret, F. Cárdenas-Lizana, M. A. Keane, Catal. Commun. 16 (2011) 159-164.

[52] M. Boronat, P. Concepción, A. Corma, S. González, F. Illas, P. Serna, J. Am. Chem. Soc. 129 (2007) 16230-16237.

[53] X. Jiang, Y. Zhang, J. Jiang, Y. Rong, Y. Wang, Y. Wu, C. Pan, J. Phys. Chem. C 116 (2012) 22619-22624.

[54] J. L. Margitfalvi, M. Hegedűs, A. Szegedi, I. Sajó, Appl. Catal. A: Gen. 272 (2004) 87-97.

[55] G. C. Bond, D. T. Thompson, Catal. Rev.-Sci. Eng. 41 (1999) 319-388.

[56] E. Bus, J. T. Miller, J. A. van Bokhoven, J. Phys. Chem. B 109 (2005) 14581-14587.

[57] I. Nakamura, H. Mantoku, T. Furukawa, A. Takahashi, T. Fujitani, Surf. Sci. 606 (2012) 1581-1585.

[58] Y. Guan, E. J. M. Hensen, Appl. Catal. A: Gen. 361 (2009) 49-56.

[59] V. Z. Fridman, A. A. Davydov, K. Titievsky, J. Catal. 222 (2004) 545-557.

[60] K. Yamaguchi, J. L. He, T. Oishi, N. Mizuno, Chem. A Eur. J. 16 (2010) 7199-7207.

[61] R. Prins, Chem. Rev. 112 (2012) 2714-2738.

[62] H. Chang, J. Phillips, Langmuir 13 (1997) 477-482.

[63] F. Cárdenas-Lizana, X. Wang, D. Lamey, M. Li, M. A. Keane, L. Kiwi-Minsker, Chem. Eng. J. 255 (2014) 695-704.

[64] P. Forzatti, L. Lietti, Catal. Today 52 (1999) 165-181.

[65] X.-H. Guan, G.-H. Chen, C. Shang, J. Environ. Sci. 19 (2007) 438-443.

[66] S. D. Jones, L. M. Neal, M. L. Everett, G. B. Hoflund, H. E. Hagelin-Weaver, Appl. Surf. Sci. 256 (2010) 7345-7353.

[67] F. Cárdenas-Lizana, B. Bridier, C. C. K. Shin, J. Pérez-Ramírez, L. Kiwi-Minsker, ChemCatChem 4 (2012) 668-673.

[68] E. Cano, C. L. Torres, J. M. Bastidas, Mater. Corros. 52 (2001) 667-676.

[69] A. Saadi, Z. Rassoul, M. M. Bettahar, J. Mol. Catal. A: Chem. 164 (2000) 205-216.

[70] B. Singh, Y. Y. Fang, B. C. C. Cowie, L. Thomsen, Org. Geochem. 77 (2014) 1-10.

[71] D. X. Liu, D. Zemlyanov, T. P. Wu, R. J. Lobo-Lapidus, J. A. Dumesic, J. T. Miller, C. L. Marshall, J. Catal. 299 (2013) 336-345.

[72] R. Maiti, A. Midya, C. Narayana, S. K. Ray, Nanotechnol. 25 (2014) 495704-pp.9.

[73] A. Retnakumari, S. Setua, D. Menon, P. Ravindran, H. Muhammed, T. Pradeep, S. Nair, M. Koyakutty, Nanotechnol. 21 (2010) 055103-pp.12.

[74] Y.-F. Han, Z. Zhong, K. Ramesh, F. Chen, L. Chen, T. White, Q. Tay, S. N. Yaakub, Z. Wang, J. Phys. Chem. C 111 (2007) 8410-8413.

[75] V. H. Vu, J. Belkouch, A. Ould-Dris, B. Taouk, J. Hazard. Mater. 169 (2009) 758-765.

[76] Y. X. Cui, X. S. Zhou, Q. Sun, L. Shi, J. Mol. Catal. A: Chem. 378 (2013) 238-245.

[77] A. B. Siqueira, E. Y. Ionashiro, C. T. de Carvalho, G. Bannach, E. C. Rodrigues, M. Ionashiro, Quim. Nova 30 (2007) 318-322.

Table 1: Physicochemical characteristics of Cu/SiO_2, Au/TiO_2 and Au/MgO.

		Cu/SiO_2	Au/TiO_2	Au/MgO
Metal loading (%w/w)		1.8	1.9	3.4
Specific surface area (SSA, $m^2\,g^{-1}$)		192	52	24
Pore volume ($cm^3\,g^{-1}$)		0.34	0.07	0.04
TPR	T_{max} (K)	545	378	510
	H_2 consumption ($\mu mol\,g^{-1}$)	281[a]/281[b]	170[a]/143[b]	5[a]/256[b]
H_2 chemisorption ($\mu mol\,g_{metal}^{-1}$)[c]		37	185	19
d (nm)[d]		3.1	3.2	7.7
Particle size range (nm)[d]		1-6	1-6	1-15

[a]experimental value obtained from TPR analysis; [b]calculated value for $Cu^{2+} \rightarrow Cu^0$ and $Au^{3+} \rightarrow Au^0$; [c]measurement at reaction temperature (498 K); [d]from STEM analysis.

Table 2: Effect of reaction temperature (*T*) and inlet (alcohol/nitroarene) molar reactant ratio (–OH/–NO_2) on imine formation rate (*R*), molar (benzaldehyde/imine) product ratio ($N_{\text{-C=O}}/N_{\text{-C=N}}$) and hydrogen utilisation efficiency (mol H_2 generated from alcohol dehydrogenation per mol imine product (H_2/–C=N)) in coupled benzyl alcohol and nitrobenzene reactions over Cu/SiO_2; *Reaction conditions*: *T* = 448-498 K, *P* = 1 atm.

T (K)	–OH/–NO_2	*R* (mmol mol_{Cu}^{-1} h^{-1})	$N_{\text{-C=O}}/N_{\text{-C=N}}$	H_2/–C=N
448	3	7	20.3	40
473	3	66	6.8	10
498	3	358	3.8	6
498	1	67	3.7	6
498	9	468	4.4	8

Table 3: Imine formation rate (*R*), molar (benzaldehyde/imine) product ratio ($N_{\text{-C=O}}/N_{\text{-C=N}}$) and hydrogen utilisation efficiency (mol H_2 generated from alcohol dehydrogenation per mol imine produced (H_2/–C=N)) as a function of Cu/Au molar ratio for coupled benzyl alcohol and nitrobenzene reactions over Cu/SiO_2 and oxide supported Au + Cu physical mixtures. *Reaction conditions*: T = 498 K, P = 1 atm, inlet alcohol/nitroarene molar ratio (–OH/–NO_2) = 3.

Catalyst	Cu/Au	R (mmol mol_{Cu}^{-1} h^{-1})	$N_{\text{-C=O}}/N_{\text{-C=N}}$	H_2/–C=N
Cu/SiO_2	-	358	3.8	6
Cu/SiO_2 +Au/TiO_2	80	609	4.4	6
Cu/SiO_2 +Au/TiO_2	20	1219	2.6	4
Cu/SiO_2 +Au/TiO_2	10	1407	2.0	3
Cu/SiO_2 +Au/MgO	20	368	4.9	6
Cu/SiO_2 +Au/MgO	10	961	2.9	4

Figure captions

Fig. 1: Reaction network in coupled benzyl alcohol and nitrobenzene reactions. *Note*: dashed arrow represents hydrogen transfer; target imine product is framed.

Fig. 2: (I) Temperature programmed reduction (TPR) profiles, **(II)** representative STEM images and **(III)** associated metal particle size distribution histograms for **(A)** Cu/SiO_2, **(B)** Au/TiO_2 and **(C)** Au/MgO.

Fig. 3: Arrhenius plots for stand-alone dehydrogenation of benzyl alcohol (■) and hydrogenation of nitrobenzene (○) over Cu/SiO_2. *Reaction conditions*: T = 423-498 K, P = 1 atm.

Fig. 4: Variation of fractional conversion (X_i, ■: benzyl alcohol, ○: nitrobenzene) with time on-stream for the coupled benzyl alcohol and nitrobenzene reactions over Cu/SiO_2. *Reaction conditions*: T = 498 K, –OH/–NO_2 = 3, P = 1 atm.

Fig. 5: Reaction rates for **(A)** dehydrogenation of benzyl alcohol and **(B)** hydrogenation of nitrobenzene over Cu/SiO_2, Au/TiO_2 and Au/MgO. *Reaction conditions*: T = 498 K, P = 1 atm.

Fig. 6: Variation of fractional conversion (X_i) and product composition (N_j) with time on-stream for the coupled benzyl alcohol and nitrobenzene reactions as a function of Cu/Au ratio (△: 10, □: 20 and ○: 80) over **(A)** Cu/SiO_2 + Au/TiO_2 and **(B)** Cu/SiO_2 + Au/MgO physical mixtures. *Reaction conditions*: T = 498 K, –OH/–NO_2 = 3, P = 1 atm.

Fig. 7: Schematic illustrating Cu-Au cooperation effect in imine production.

Fig. 8: XPS spectra: **(A)** C1*s* and **(B)** Cu $2p_{3/2}$ **(I)** *pre*- and **(II)** *post*-reaction over Cu/SiO_2 and **(III)** after reaction over Cu/SiO_2 + Au/TiO_2; experimental data are given by □ where lines represent the fits with peak deconvolution.

Fig. 9: (A) TGA profiles for catalysts *pre*-reaction (solid lines: **(I)** Cu/SiO_2; **(II)** Cu/SiO_2 + Au/TiO_2) and *post*-reaction (dashed lines: **(III)** Cu/SiO_2; **(IV)** Cu/SiO_2 + Au/TiO_2). Inset Table: elemental (C and H) analysis. **(B)** DSC analysis of Cu/SiO_2 (solid line) and Cu/SiO_2 + Au/TiO_2 (dashed line) *post*-reaction.

Fig. 1

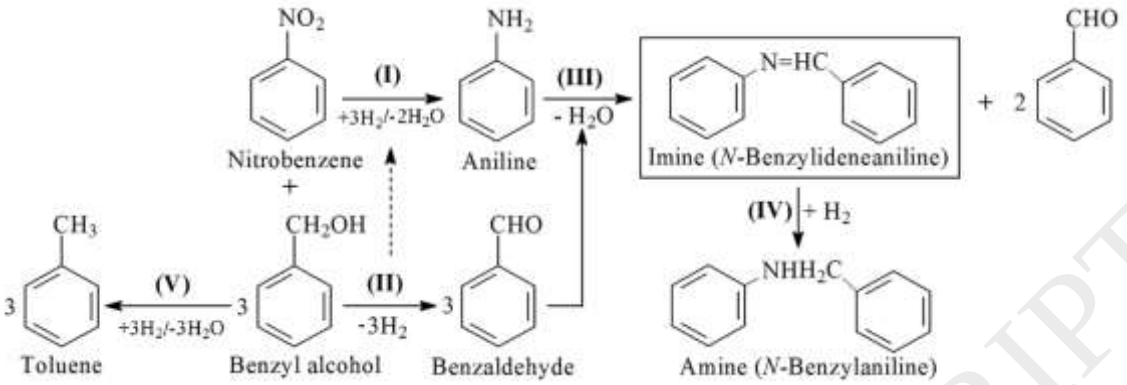

Fig. 2

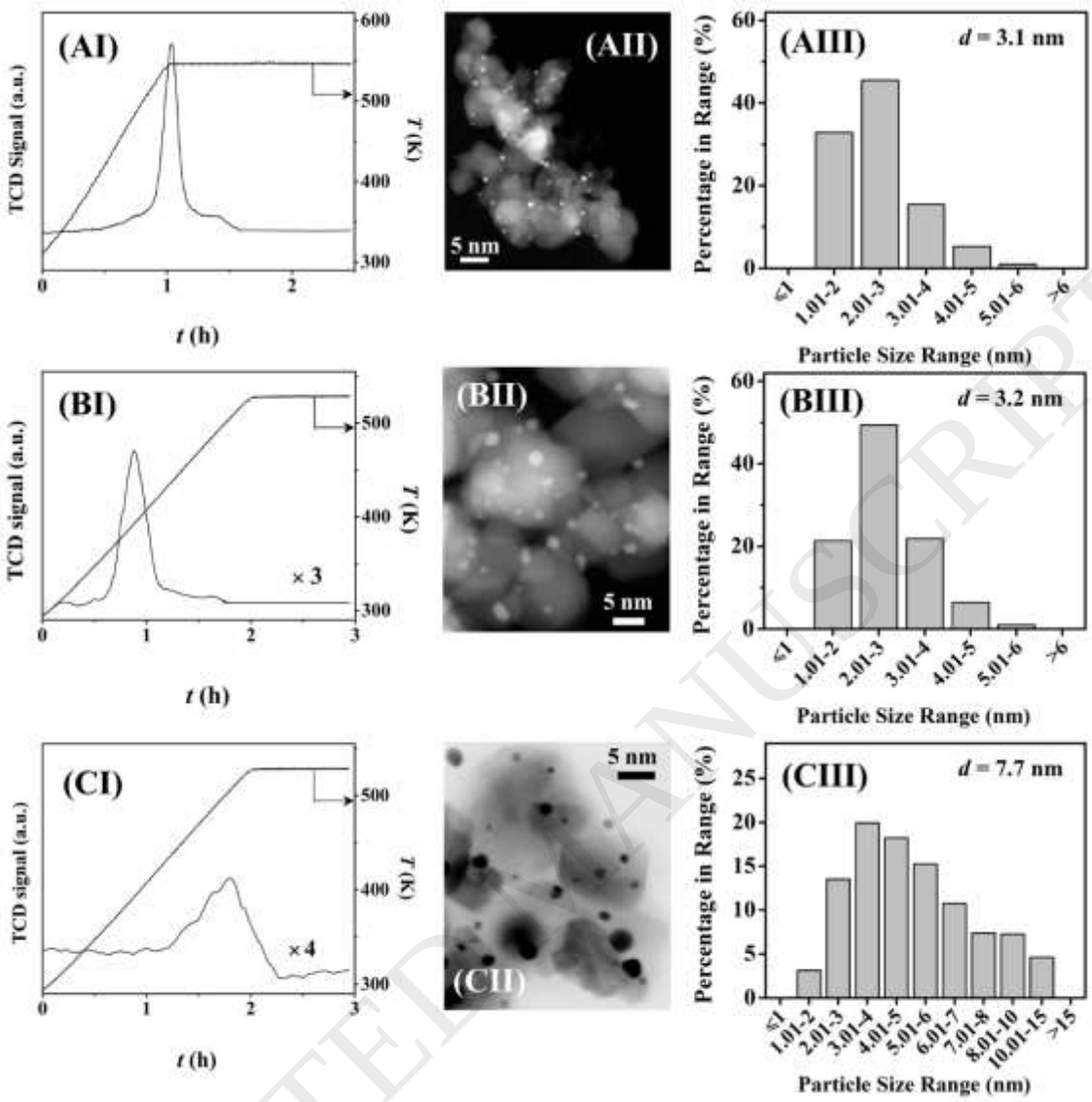

Fig. 3

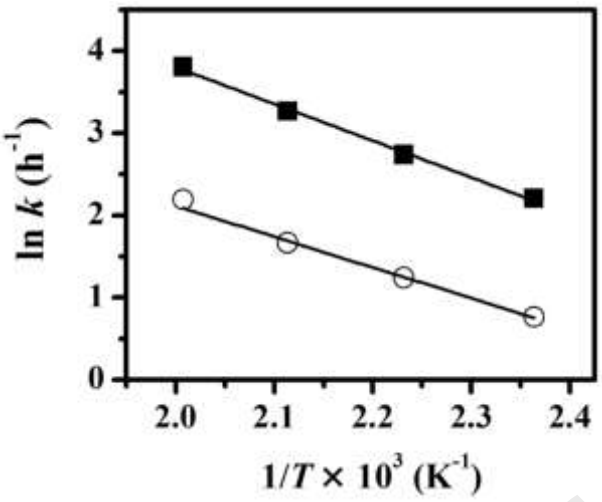

Fig. 4

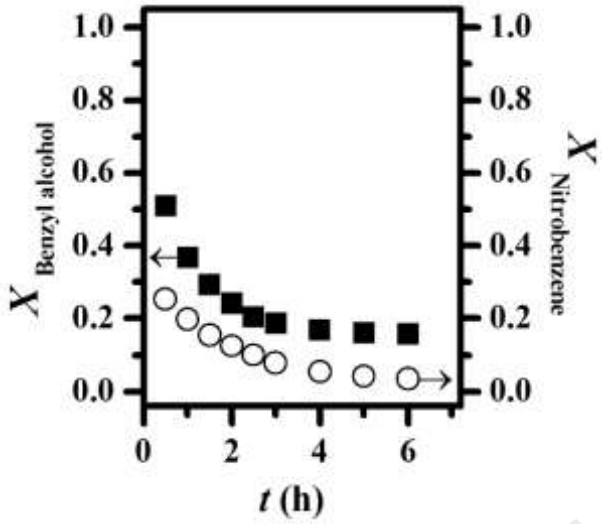

Fig. 5

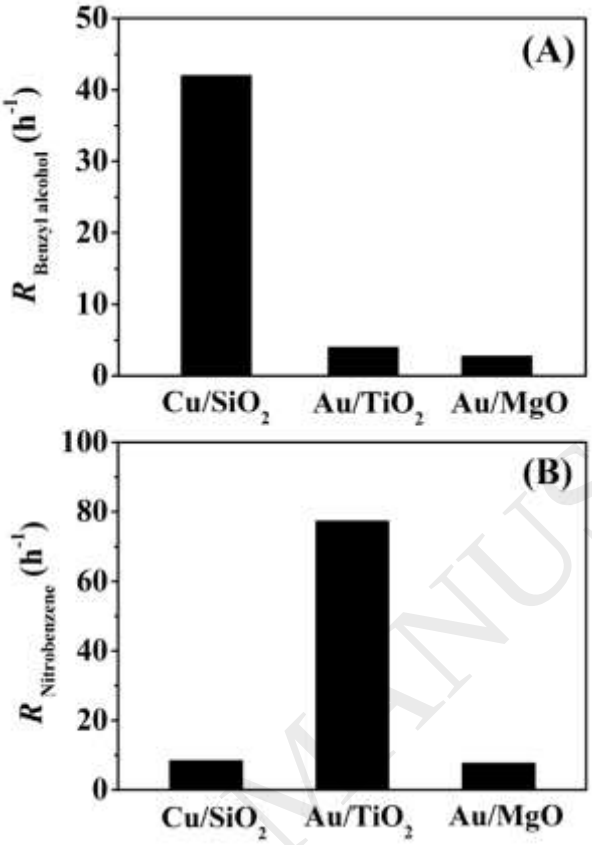

Fig. 6

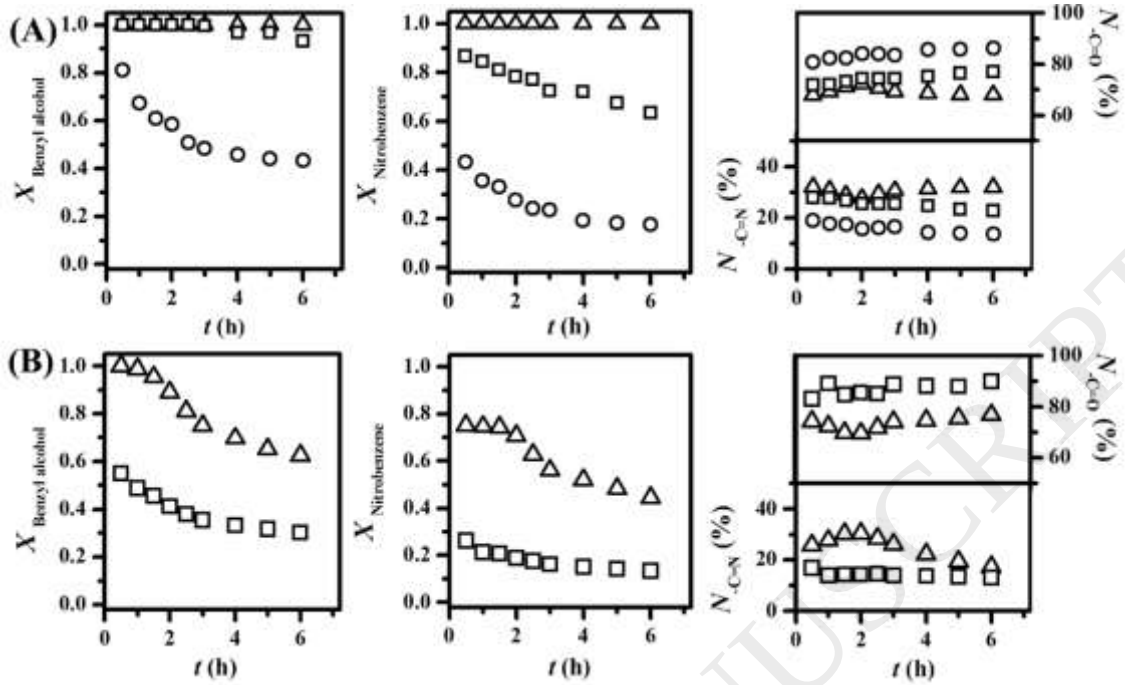

Fig. 7

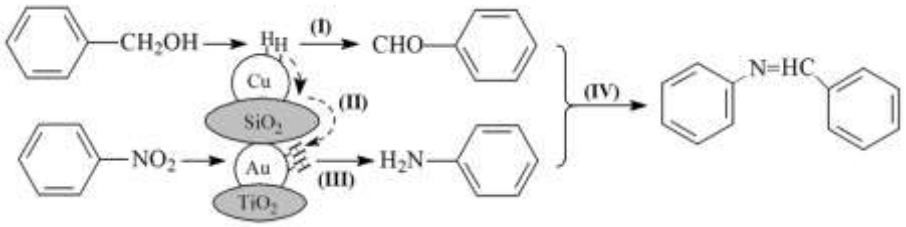

Fig. 8

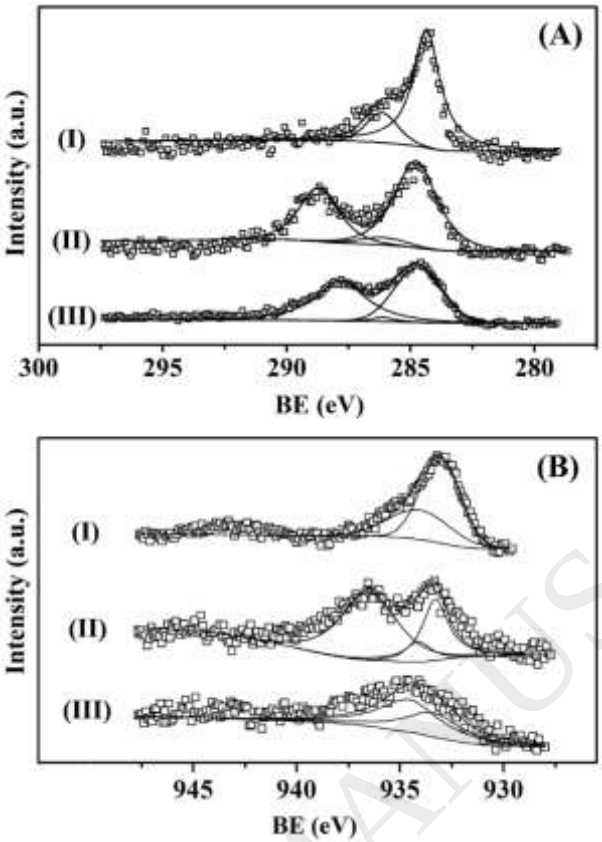

Fig. 9